© 2021. Published by The Company of Biologists Ltd | Development (2021) 148, dev196519. doi:10.1242/dev.196519

RESEARCH ARTICLE

Hydrostatic mechanical stress regulates growth and maturation of the atrioventricular valve

David Bassen*, Mingkun Wang*, Duc Pham, Shuofei Sun, Rashmi Rao, Rishabh Singh and Jonathan Butcher‡

ABSTRACT

During valvulogenesis, cytoskeletal, secretory and transcriptional events drive endocardial cushion growth and remodeling into thin fibrous leaflets. Genetic disorders play an important role in understanding valve malformations but only account for a minority of clinical cases. Mechanical forces are ever present, but how they coordinate molecular and cellular decisions remains unclear. In this study, we used osmotic pressure to interrogate how compressive and tensile stresses influence valve growth and shape maturation. We found that compressive stress drives a growth phenotype, whereas tensile stress increases compaction. We identified a mechanically activated switch between valve growth and maturation, by which compression induces cushion growth via BMP-pSMAD1/5, while tension induces maturation via pSer-19-mediated MLC2 contractility. The compressive stress acts through BMP signaling to increase cell proliferation and decrease cell contractility, and MEK-ERK is essential for both compressive stress and BMP mediation of compaction. We further showed that the effects of osmotic stress are conserved through the condensation and elongation stages of development. Together, our results demonstrate that compressive/tensile stress regulation of BMP-pSMAD1/5 and MLC2 contractility orchestrates valve growth and remodeling.

KEY WORDS: Mechanobiology, Cardiac valve development, BMP signaling, MLC contractility

INTRODUCTION

Congenital heart defects (CHDs) are the most common birth defects and the leading cause of infant death due to birth defects, affecting 0.5-2.0% of the general population (Virani et al., 2020; Gilboa et al., 2016). Heart valve malformation accounts for over 25% of all CHDs (Van Der Linde et al., 2011; Hoffman, 2013). Valve formation is a multistep process that relies on multiple signaling pathways acting in a spatiotemporally coordinated manner. Although the regulatory events initiating this process are well known, their clinical impact has been limited in part because failure to initiate valve formation is almost uniformly lethal in early gestation (Srivastava, 2006). Clinically serious malformations arise instead from improper growth and maturation of the valvular cushions into thin fibrous leaflets (Nishimura et al., 2014). However, mechanistic understanding of these later events is limited. Given the clinical importance of proper valve morphogenesis, identification of mechanisms coordinating developmental pathways is imperative.

Throughout valve development, flowing blood directly and indirectly generates various forces that have crucial effects on developmental programs. Initially, shear stress promotes endothelial-to-mesenchymal transition (EndMT) to form the endocardial cushions. As EndMT subsides, the cushions continue to grow as cells proliferate. This leads to a constriction of the lumen, resulting in a higher shear stress and compression-dominated mechanical environments. At later stages, cushions elongate and thin to become mature valves with stratified and aligned cells and matrix. The thinning structure and unidirectional flow create a mechanical environment dominated locally by complex shear stresses and tension. It has been well demonstrated that disrupting stress environments generated by physiological flow will lead to defective valve development (Hove et al., 2003). However, the role of stress environments in coordinating molecular and cellular decisions remains incompletely understood. Many studies and our previous work show that shear stress and cyclic stretch can regulate important developmental pathways, but studies of compressive and tensile stress are lacking (Yalcin et al., 2011; Buskohl et al., 2012a).

Here, we have interrogated the roles of tensile and compressive stress in valve growth and shaping by modulating osmotic pressure. Osmotic stress is a long-established method for studying the mechanosensitive response in soft tissues, organoids and spheroids that are too small and amorphous to secure on a traditional testing device (Basser et al., 1998; Chevalier et al., 2016). The hyper-osmotic stress creates compressive loads by inducing a net outward flow of water from the tissue and the underlying cells, while hypo-osmotic stress has been used to create tensile loads by inducing a net inward flow of water into the tissue and into the underlying cells. We applied these loads in a hanging drop culture system to isolate explants from surfaces that would induce migration or apply additional traction forces (Buskohl et al., 2012a). In this study, we demonstrated that mechanical stresses induced by osmotic stress can alter cushion size through changes in contractile and proliferative behaviors. We further identified a mechanically activated switch between valve growth and maturation, by which compression induces cushion growth via BMP-pSMAD1/5 while tension induces maturation via pSER-19-mediated MLC2 contractility.

RESULTS

We used the avian (chick) model, due to its low cost and to the ease of obtaining large numbers of fresh tissue and cells at stages of interest from eggs within a short period. Chick and quail models are well-established tools for studying development (Kain et al., 2014). The four-chambered avian heart develops in a manner that mirrors that of the human heart (Aikawa et al., 2006). Here, we isolated fresh HH25 cushions and cultured them in a hanging drop (one per drop) for 24 h (Fig. 1A). Compressive stress (hypertonic) conditions were applied by adding 0.14 M sucrose to the media (increasing

The Nancy E. and Peter C. Meinig School of Biomedical Engineering, Cornell University, Ithaca, NY 14853, USA.
*These authors contributed equally to this work

‡Author for correspondence (jtb47@cornell.edu)

J.B., 0000-0002-9309-6296

Handling Editor: Thomas Lecuit
Received 3 September 2020; Accepted 26 May 2021

Development (2021) 148, dev196519. doi:10.1242/dev.196519

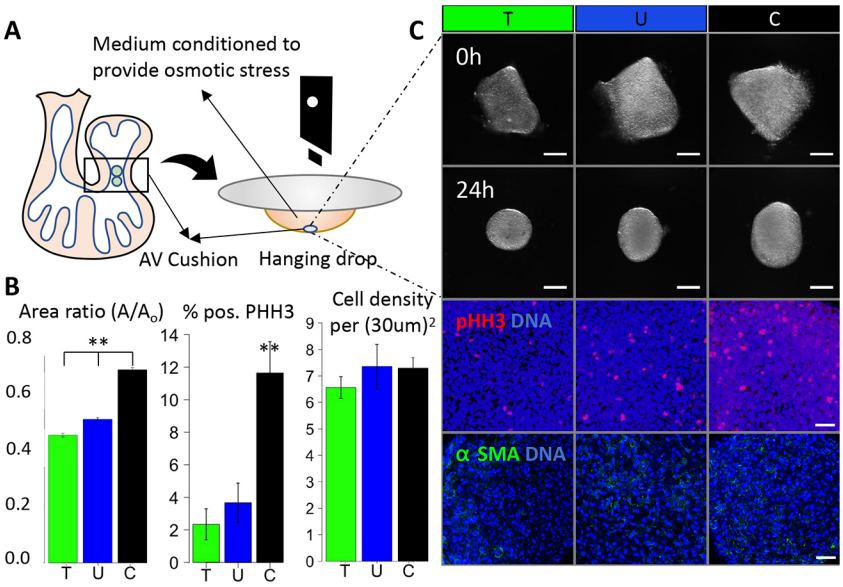

Fig. 1. Osmotic pressure regulates the cushion compaction phenotype *in vitro*. (A) Schematic of experimental design. (B) Compaction (24 h), proliferation (10 h) and cell density (24 h) of HH25 AV cushions cultured in conditioned media. (C) Endpoint bright-field and immunofluorescence images of HH25 AV cushions compacting and rounding over 24 h of hanging drop culture. T, tensile stress; U, unloaded; C, compressive stress. Scale bars: 200 µm in bright-field images; 0.25 µm in immunofluorescence images. *n*=4-6 cushions per condition from 3-6 independent experiments; data are mean±s.e.m. ***P*<0.01 (ANOVA with Tukey's post-hoc test).

osmolarity by 54%), while tensile stress (hypotonic) was achieved by reducing the base media by 50% (decreasing osmolarity by 40%). We refer to the osmotically balanced media control as the unloaded condition (U).

Compressive/tensile stress regulates the cushion compaction phenotype *in vitro*

At 24 h, all tissues have compacted significantly, as measured by area ratio (Fig. 1B), but compressive loaded cushions had the largest area and tensile loaded cushions had the smallest. All cushions rounded from a trapezoidal shape into a circular or elliptical shape (Fig. 1C). We confirmed that cushions were viable in loaded and unloaded conditions at 24 h. Proliferation increased with compressive stress compaction, but osmotic stress did not significantly affect cell density (Fig. 1B) or apparent tissue stiffness (Fig. S1).

Compressive stress regulates tissue compaction through BMP signaling

To reveal the mechanism of how osmotic stress induces cushion compaction, we first examined if TGFβ was being activated by compressive stress (Buskohl et al., 2012b). TGFβ treatment could drive a growth phenotype (Fig. S2B). TGFβ signaling is initiated by TGFβ1, TGFβ2 and TGFβ3, and primarily through Smad activation. Specifically, several Smads, including Smad2 and Smad3 will be phosphorylated by TGFβ receptors, forming Smad2/3 complexes and translocating into the nucleus. However, here we found no significant differences in pSmad2/3 nuclear localization between osmotic treatments (Fig. S2C). Furthermore, Alk5/7 inhibitor SB431542 (2.6 µM), which blocks TGFβ2 and TGFβ3 signaling, did not alter the effects of compressive stress with confirmed successful inhibition of Smad2/3 phosphorylation (Fig. S2A).

Given the role of BMPs in valve maturation, but unclear role in growth-related mechanosensitive mechanisms, we examined the role of BMP signaling as an alternative to the TGFβ pathway (Beppu et al., 2009). During the compaction, we found significant differences in pSmad1 and pSmad5 nuclear localization, with compressive stress showing the highest pSmad1 and pSmad5 activity, suggesting elevated BMP signaling (Fig. 2A). Alk2 and Alk3 inhibitor LDN significantly enhanced osmotic stress induced compaction (Fig. 2B). We used BMP treatment to simultaneously explore the direct role of BMP in cushion remodeling and as an agonist of the pSmad1and pSmad5 pathway. We found that BMP treatment (20 ng/ml) markedly decreased compaction without affecting rounding (Fig. 2C). As expected, such an effect of BMP on cushion compaction was blocked by co-treatment with the Alk2 and Alk3 inhibitor LDN.

Compressive stress-driven cushion growth requires MEK-ERK

Additionally, we investigated a potential downstream kinase pathway of BMP, MAPK MEK-ERK, which is implicated in mechano-signaling and mediation of Smad1 and Smad5 signaling

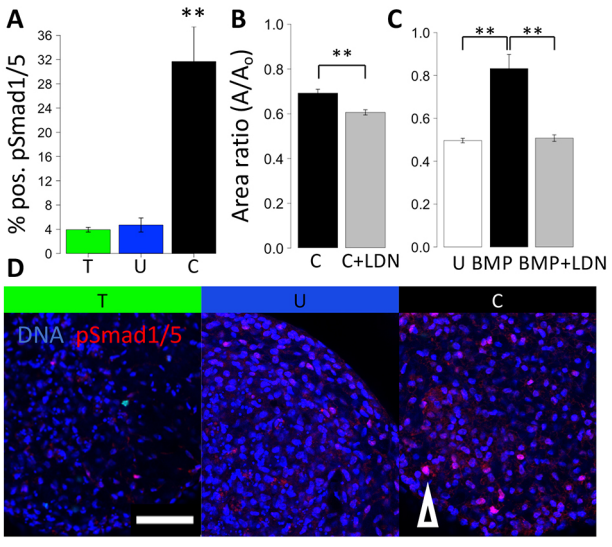

Fig. 2. Compressive stress regulates tissue compaction through BMP signaling. (A) Percentage of cells positive for pSmad1 and pSmad5 in HH25 cushions cultured under osmotic stress for 24 h, *n*=4 or 5, data are mean±s.d. (B) Compaction trend for compressive stress combined with the Alk2/3 inhibitor LDN. (C) Compaction trend for BMP treatment combined with the Alk2/3 inhibitor LDN, *n*=4 or 5 cushions per condition, data are mean±s.e.m. (D) Representative immunofluorescence images stained for pSmad1/5 of HH25 cushions cultured under osmotic stress over 24 h. T, tensile stress; U, unloaded; C, compressive stress. Arrowhead indicates an example of a pSmad1/5-positive cell. Scale bar: 50 µm, ***P*<0.01 [ANOVA with Tukey's post-hoc test (A,C) and a two-tailed unpaired *t*-test (C)].

Development (2021) 148, dev196519. doi:10.1242/dev.196519

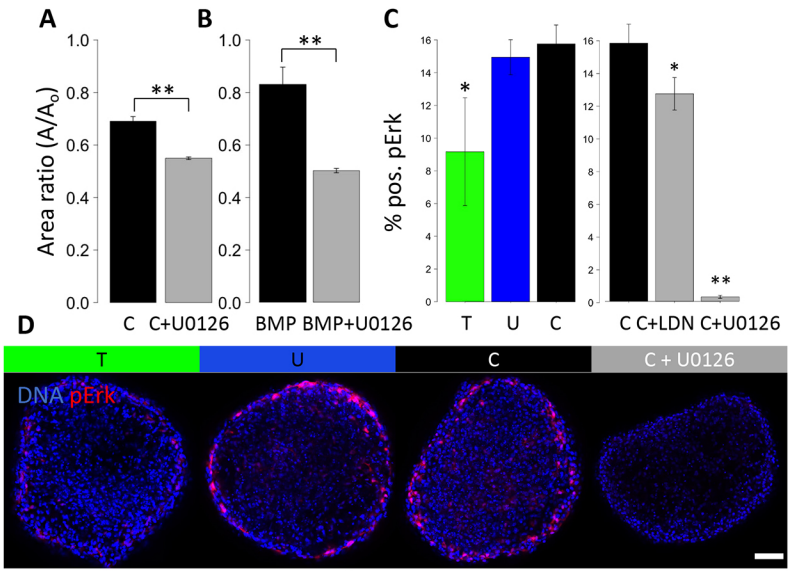

Fig. 3. MEK-ERK is involved in the tissue growth driven by BMP and by compressive stress. (A) Compaction trend for compressive stress combined with the MEK inhibitor U0126. (B) Compaction trend for BMP treatment combined with the MEK inhibitor. (C) Percentage of cells positive for pERK in HH25 cushions cultured under osmotic stress, and cultured with BMP and MEK inhibitors. (D) Representative immunofluorescence images stained for pERK of HH25 cushions cultured under osmotic stress and cultured with a MEK inhibitor. T, tensile stress; U, unloaded; C, compressive stress. Scale bar: 50 µm, *n*=4-6 cushions per condition per three independent experiments, data are mean±s.e.m., **P*<0.05, ***P*<0.01 [ANOVA with Tukey's post-hoc test (C) and a two-tailed unpaired *t*-test (A,B)].

(Zhou et al., 2013). MEK inhibition via U0126 has a large effect on the growth phenotype, significantly blocking the effect of compressive stress (Fig. 3A) and completely blocking BMP (Fig. 3B). We examined ERK activation at 24 h and 18 h to assess an intermediate time point during remodeling compaction. At 18 h, p-ERK is not significantly elevated in the compressive condition, but is clearly blocked successfully by MEK inhibition, and slightly by Alk2 and Alk3 inhibition (Fig. 3C).

Tensile stress induces tissue compaction through non-muscle myosin II-mediated cell contractility

To assess a contractile mechanism for osmotic and BMP growth phenotypes, we first used blebbistatin treatment and found a dose-dependent effect on tissue size, and that tissue compaction was inhibited at lower doses of blebbistatin (1 µM) and was reversed at a higher dose (at or beyond 2 µM) (Fig. 4A). However, inhibition of ROCK using Y27362 led to a modest, statistically insignificant reduction in compaction when applied to the unloaded condition and did not affect tissue rounding (Fig. 4B). Blebbistatin treatment could also block tissue rounding partially at 1 µM and completely at 2 µM. To determine whether there was a role for ROCK as an upstream kinase for contractile signaling, we stained for RhoA-GTP. We found Rho activity localized to the endothelial cells during compaction (Fig. S3A). ROCK inhibition disrupted endothelial polarity, resulting in clumped and disorganized surface cells (Fig. S3B). We also observed honeycomb-like RhoA-GTP staining patterns in the cytoplasm of cells under compressive stress (Fig. S3B).

Next, non-muscle (NM) myosin II activation was assessed by staining for p-SER19 on the NM myosin II light chain. pSER-19 decreased significantly in both the compressive and tensile conditions (Fig. 4C). We then assessed the myosin activity when directly applying BMP ligand. BMP treatment significantly reduced SER-19 activation, which could be restored slightly by LDN or significantly by MEK inhibition.

Sustained compression upregulates BMP signaling and impairs valve thinning *in vivo*

We performed partial atrial ligation experiments on *ex ovo* cultured chick embryos to determine the morphogenetic impact of altered compressive/tensile stress environments on valvulogenesis *in vivo*. Left atrial ligation (LAL) is a method to surgically reduce the hemodynamics placed on the atrioventricular valve (Midgett and

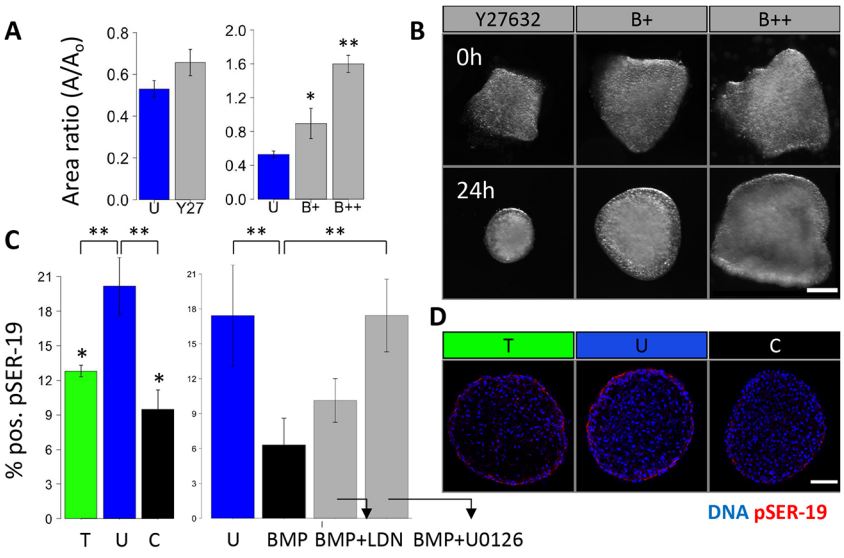

Fig. 4. NM-myosin-II is inhibited in tissue growth driven by BMP and by compressive stress. (A) Compaction of HH25 AV cushions cultured with the ROCK inhibitor Y27632, 1 µM NM myosin II inhibitor blebbistatin (B+) and 10 µM blebbistatin (B++) for 24 h. (B) Representative images of cushions treated with blebbistatin showing varying degrees of compaction and rounding. (C) Percentage of pSER19-positive cells in HH25 cushions cultured under osmotic stress, and with BMP, the BMP inhibitor LDN and the MEK inhibitor U0126 for 24 h. (D) Representative immunofluorescence images stained for pSER19 of HH25 cushions cultured under osmotic stress over 24 h. Scale bars: 50 µm, *n*=4-6 cushions per condition per three independent experiments, data are mean±s.e.m., **P*<0.05, ***P*<0.01 (ANOVA with Tukey's post-hoc test).

Development (2021) 148, dev196519. doi:10.1242/dev.196519

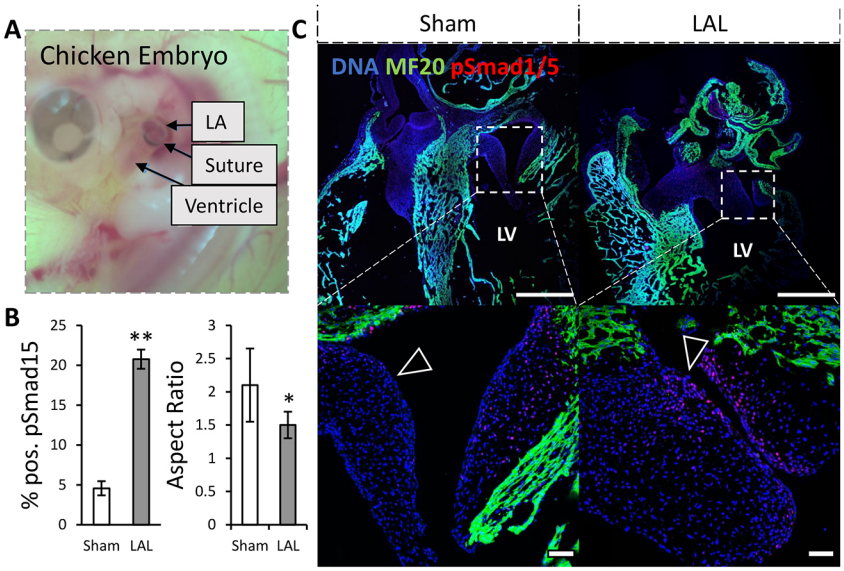

Fig. 5. Altered mechanical loading upregulates BMP signaling and impairs valve thinning *in vivo*. (A) Photo showing left atrial ligation of the chicken embryo heart. (B) Number of cells positive for pSmad1 and pSmad5, n=3 sections from independent embryos per condition, data are mean±s.d. (C) Immunohistochemical images of HH30 chick mitral valve stained for pSmad1 and pSmad5 and MF20 (myocardial marker) with arrowheads indicating location on the atrial aspect with increased pSmad1 and pSmad5 signaling under LAL. Scale bars: 100 µm, LV, left ventricle; LA, left atrium, *P<0.05, **P<0.01 (two-tailed unpaired t-test).

Rugonyi, 2014; Sedmera et al., 1999) (Fig. 5A). Under LAL, the mitral septal leaflets were significantly less elongated at day 7, when compared with sham control, indicated by a smaller aspect ratio (Fig. 5B). As anticipated from our results, delayed tensile stress environment enhanced the expression of pSmad1 and pSmad5 in LAL leaflets. The mural leaflets generally showed high pSmad1 and pSmad5 activity with a statistically insignificant increase in the LAL condition.

Compressive and/or tensile stress promotes spatially coordinated Smad1, Smad5, ERK and myosin activity

We found significant differences in the spatial localization of the pSmad, pERK and pSER-19 signals within the cushion. pSmad1 and pSmad5 activation was observed throughout the outside and inner layers of the cushions when expressed. Compressive stress resulted in higher pSmad1 and pSmad5 activity throughout the cushion (Fig. 6A) that also correlated with greater expression near the tissue surface. pERK activity was present across the cushions (Fig. 6B). We found that pERK activity occurred in all conditions around a mean normalized radius of 0.8, which corresponds to a sub-endocardial region. We found that pSER-19 was present at or near the surface layers of the cushion, and compressive stress resulted in a decrease in pSER-19 activity throughout the surface layers (Fig. 6C,D). The mean normalized radius of pSER-19-positive cells was at or above 0.9 for all conditions.

Compressive/tensile stress regulates growth and compaction across stages of valve development

To determine the relative contributions of the extracellular matrix (ECM) and cell contractility in determining cushion shape, we

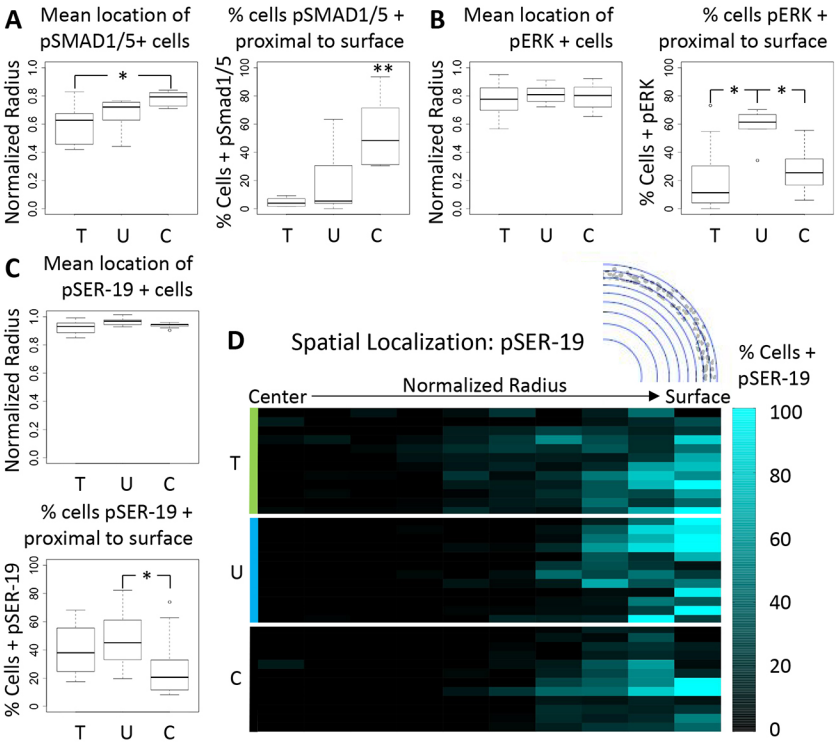

Fig. 6. Smad1/5, ERK and myosin activity are spatially coordinated in response to osmotic stress. (A) The mean normalized radii for pSmad1- and pSmad5-positive cells in HH25 cushions cultured under osmotic conditions, and percentage of signal at or near the cushion surface. (B,C) The same scenarios are shown for pERK-positive cells (B) and pSER19-positive cells (C). Lines within boxes indicate the median. The length of each box represents the interquartile range. The whiskers indicate the highest and lowest observed values (unless outliers, which are indicated by points). (D) Color map of pSmad1 and pSmad5 distribution along a normalized cushion radius within 10 regions of interest of equal area. n=3-8 cushions per group with two slices per cushion around 30 µm. T, tensile stress; U, unloaded; C, compressive stress. *P<0.05, **P<0.01 (ANOVA with Tukey's post-hoc test).

Development (2021) 148, dev196519. doi:10.1242/dev.196519

assessed cushion compaction under osmotic loads at mid to late stages of development where collagen matrix begins to dominate (Butcher et al., 2007). Cushions in unloaded conditions compacted across all stages, from HH25 to HH36, by 50%, even given an increasing collagen matrix density, until after HH40, where compaction stops at 80% (Fig. 7A). Cushions in hypotonic conditions compact 10% more than controls, an effect that diminishes at later stages. Cushions in compressive stress conditions compact between 70 and 80% across all stages. Degradation of collagen matrix via collagenase II in HH40 leaflets led the leaflets to compact by 50% over 24 h, as in unloaded cushions at HH25. Collagenase treatment also led to a loss in the thin, saddle-like morphology of HH 40 leaflets (Fig. 7B). Interestingly, the HH40 leaflets still retained an elongated axis with the same aspect ratio as HH34 leaflets, even though collagenase treatment resulted in a decrease of tissue stiffness. The strain energy densities decreased from about 3 Pa to around 0.4 Pa.

Despite the increased collagen matrix content preventing leaflet compaction, we still found a generally higher pSER-19 activity at later stage (HH40) compared with mid stage (HH25). Overall, the percentage of positive pSER-19 cells was above 20% but there was no significant difference among different loading conditions (Fig. 7D). The nuclear localization of pSmad1 and pSmad5 was less than 4% and generally less than that number if mid-stage; again, there was no significant difference between the loading conditions (Fig. 7C). As for HH25, spatial distribution of pSER at HH40 was also localized mainly near the surface (Fig. 7F), but the distribution of pSmad was scattered across the width (Fig. 7G). Another finding is the anisotropic distribution of pSER-positive cells under compressive and unloaded loads. By measuring the angle between the long axis (perpendicular to elongating direction) and the lines drawn by positive pSER cells, we found, under compressive and unloaded conditions, that pSER-positive cells were located mainly in the endothelium and distributed along tissue edges, while pSER-positive cells under the tensile stress condition were located in the subendothelial region and aligned roughly in the direction parallel to the long axis (Fig. 7H,I), suggesting endothelial cells could not generate enough compaction while interstitial cells became a driver in tension-induced tissue compaction.

DISCUSSION

Long-term physiological valve function requires that fetal valve primordia morph into leaflets with the correct shape and size to maintain one-way blood flow through the heart. Understanding how mechanically driven signals and processes influence the outcome of valve morphogenesis first requires clarifying the role of individual stimuli. Using osmotic stress to mimic the compression and tension-loading environments *in vivo*, we found that compression promotes cushion growth, while tension promotes cushion remodeling and leaflet thinning. We further identified BMP as a mechanosensitive driver of valve growth and mid-stage development, and this pathway involves the regulation of NM myosin activity through cooperation with MEK-ERK signals. During late-stage development, the mechanical environment changes dramatically from a compression-dominated environment to a tension-dominated environment, the activation of BMP-SMAD1/5 or NM myosin activity switched in response to such mechanical environment change.

To induce the compressive/tensile stress, we used sucrose to mediate the osmolarity of culture media. To demonstrate that the influence of sucrose on cushion growth was indeed through osmotic stress, we compared the cell proliferation in cushions cultured in

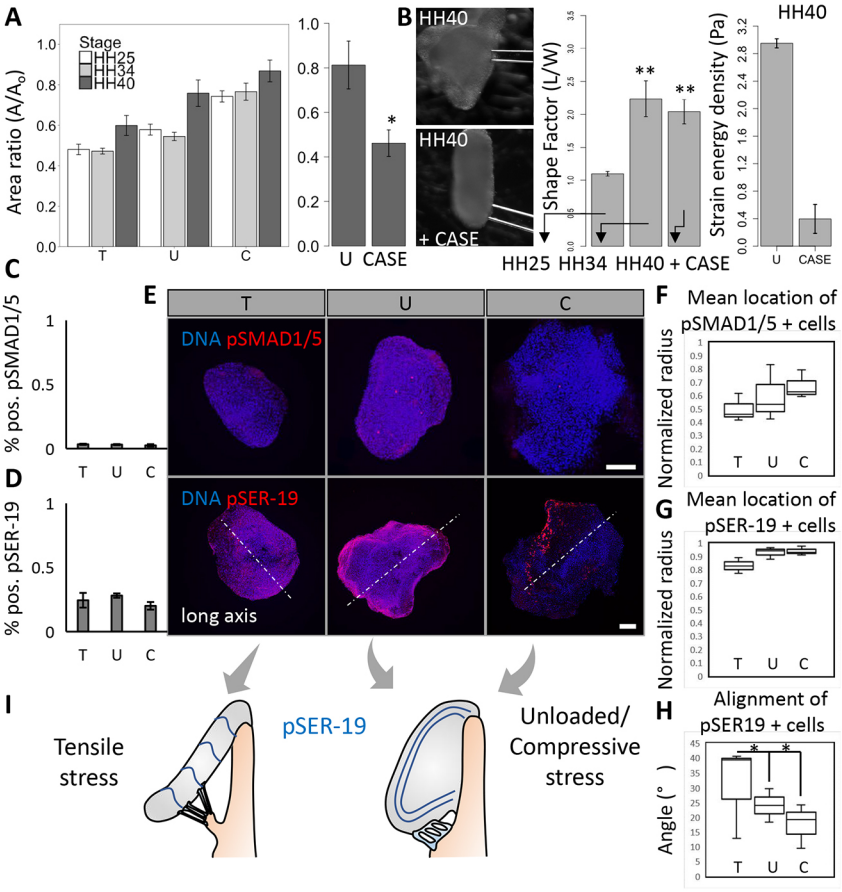

Fig. 7. Compressive/tensile stress-regulated tissue compaction is conserved across stages of valve maturation and its interaction with extracellular matrix preserves leaflet morphology. (A) The compaction behavior of cushions across mid to late stages under osmotic stress conditions, and across late stage (HH40) compaction with collagenase II treatment (300 U). (B) Wide-field images of a HH40 leaflet before and after 24 h treatment with collagenase II (CASE). Shape factors, measured as aspect ratio, of HH25 and HH34 cushions cultured for 24 h, and HH40 leaflets cultured with collagenase II for 24 h. n=4-6 cushions per condition per three independent experiments, data are mean±s.e.m. Strain energy densities for control/unloaded and collagenase treated HH40 leaflets, three or four cushions per condition, data are mean±s.d. Percentage of pSmad1- and pSmad5- (C), and pSER19- (D) positive cells in HH40 leaflets cultured under osmotic stress for 24 h, n=3 leaflets per condition, data are mean±s.d. (E) Representative 3D reconstructed immunofluorescence images stained for pSmad1 and pSmad5, and pSER19 of HH40 leaflets cultured under osmotic stress over 24 h. The mean normalized radii for pSmad1- and pSmad5- (F), and pSER19- (G) positive cells in HH40 leaflets cultured under osmotic stress, n=3 leaflets per condition. (H) Angle between aligned pSER19-positive cells and long axis (perpendicular to elongation direction), n=3. Lines within boxes indicate the median. The length of each box represents the interquartile range. The whiskers indicate the highest and lowest observed values (unless outliers, which are indicated by points). (I) Schematic of alignment of pSER19-positive cells in HH40 leaflets under compressive/tensile stress and unloaded conditions. Scale bars: 100 µm. *P<0.05, **P<0.01.

Development (2021) 148, dev196519. doi:10.1242/dev.196519

hypertonic sucrose media to cushions cultured in hypertonic NaCl media. These two media had the same osmolarity and similar percentages of pHH3-positive cells (Fig. S7A), confirming that hypertonicity promotes cell proliferation. In a second experiment, we treated cushions with hypertonic and unstressed media containing the same amount of sucrose. The results show higher osmolarity led to a significantly higher percentage of pHH3-positive cells (Fig. S7B), suggesting that other potential effects from sucrose addition, such as metabolic uptake, did not significantly impact cushion growth.

It is well appreciated that TGFβ and BMP signaling control cellular activities associated with tissue growth, but rarely have the full multi-scale molecular, cellular and tissue level interactions been interrogated in the same study. Furthermore, how these pathways are coordinated to activate and/or suppress remained elusive. We establish here that BMP signaling is an essential inducer/mediator of AV valve growth during mid-stage development. Interestingly, we previously found that TGFβ3 also increased AV valve tissue size, but here determined that TGFβ signaling via pSmad2 and pSmad3 was dispensable for mechanically induced growth. Given the studies showing a key role for TGFβ and Smad2/3 in regulating EndMT during early cushion formation (Gould et al., 2016), the contribution of TGFβ signaling to valve development may change with stages, possibly owing to the dramatic change of mechanical environments. On the other hand, pSmad1 and pSmad5 was upregulated by compressive stress in combination with a reduction in tissue size with the application of an Alk2 and Alk3 inhibitor. This supports TGFβ and BMP as independent mediators of compaction; however, BMP is uniquely activated by compressive stress. *In vitro*, BMP2 treatment alone was found to produce a similar growth phenotype. *In vivo*, aberrant BMP signaling has been associated with deficient or hyperplastic valves in newborn mice lacking epidermal growth factor receptor (EGFR) or tumor necrosis factor-a converting enzyme (TACE) (Jackson et al., 2003). Such studies using genetically mutated mice show that disruption of BMP signaling can also be independent of compressive stress. During natural development, BMP signaling is regulated by forces generated by blood flow, but genetic abnormalities can disrupt the natural regulatory process. In addition to the widely recognized role of BMP signaling in cell proliferation, we found here that the compression activation of BMP, Smad1 and Smad5 can drive cushion growth by limiting cell contractility. In fact, BMP has different downstream signaling depending on the upstream input. For example, during EndMT myocardial BMP signaling can promote the breakdown of endocardial cell-cell contact by upregulation of Snail1 and Snail2 (Ma et al., 2005; Rivera-Feliciano and Tabin, 2006). These contextual differences of BMP signaling highlight the importance of upstream coordination: a deliberate coordination is required for valve growth and maturation. Mechanical coordination can provide such tunability because mechanical inputs will converge as valves develop to match the same biomechanical demand. This could explain how valves with very different sizes can end up in the same tightly controlled anatomical morphology.

Our results also show that valve morphogenesis requires precise spatial coordination between pSmad1, pSmad5 and pERK: their colocalization in the same cell or neighboring cells may be required for the inhibition of NM-myosin activity and thus cell contractility. We confirmed that the surface layer of cells around the cushion was where endothelial cells remained on the surface by examining the spatial distribution of the endothelial marker VE-cadherin (Fig. S6). Given that pSER-19 was present at or near the surface of the cushion, while pSmad1 and pSmad5 were observed throughout the cushions, endothelial contractility and mesenchymal proliferation may play distinct roles in driving the cushion growth [previous studies only considered the role of endothelial cells in tissue shaping (Ninomiya and Winklbauer, 2008; Hughes et al., 2018)]. Furthermore, our data show a signaling crosstalk between endocardial and mesenchymal cells during cushion compaction. We found that colocalization of pERK, pSmad1 and pSmad5 in the sub-endocardial region may synergize to regulate the endocardial cell contractility, suggesting mesenchymal BMP, Smad1 and Smad5 could affect endocardial cell contractility. Given the studies proposing that endocardial Notch1 limits mesenchymal BMP signaling and subsequent mesenchymal proliferation by activating heparin-binding EGF-like growth factor (HBEGF) (MacGrogan et al., 2016), a closed loop of interactions between endocardial and interstitial mesenchymal cells may exist.

This work showed the existence of a molecular switch by which compression promoted cushion growth through BMP, pSmad1 and pSmad5 while tension promoted valve maturation by upregulation of pSER-19-mediated cell contractility. We previously reported a FilGAP-regulated switch in valve growth and remodeling, which is activated by cyclic stretch to turn on RhoA or Rac1 pathway (Gould et al., 2016). The acute cyclic stretch activated RhoA to produce a myofibroblast phenotype, while chronic cyclic stretch activated Rac1 to drive matrix compaction for valve maturation. These two studies lead to a hypothesis that different mechanical signaling regulates different signaling coordination, probably through a transition at molecular level. Such molecular level 'switching' relationship between BMP, pSmad1 and pSmad5 and pSER-19-mediated cell contractility is common during tissue development. Another example in heart development is the ability of the Hippo pathway to restrict heart size, while the nuclear translocation of YAP can activate cardiac growth (Wang et al., 2018). YAP is now widely acknowledged to be a mechanosenstive transcription factor that can be activated independently of canonical Hippo signaling.

The transition from growth program to maturation program is associated with a transition from compression-dominated environments to tension-dominated environments. Cushions were subjected to compression-dominated environments when growing thicker. Although at later stages, with elongation and thinning of cushions, tensile stress became dominated. Our study suggests this mechanical transition orchestrates cushion growth and maturation via signaling coordination between BMP, pSmad1 and pSmad5 and MLC2 cross endothelial and mesenchymal cells. Several mechanosensing mechanisms may be involved in the transduction of compressive and/or tensile stress, such as YAP and/or TAZ and mechanically gated ion channels. These different mechanisms may activate different signaling pathways in response to mechanical environments. The impact of mechanical stimuli may also depend on whether the stresses are transduced at the cell membrane or the cytoskeleton. Disrupted compressive and/or tensile stress sensing could result in defective growth and/or maturation, eventually leading to the malformation of heart valves. This concept provides a possible answer to a long-standing question of why only a small minority of CHDs have an identifiable genetic cause. Many clinically serious CHDs, such as tetralogy of Fallot and persistent truncus arteriosus, and prevalent but variably mild forms, such as ventricular septal defect, are the result of defective cushion growth in outflow tract (Lindsey et al., 2014). Our hypothesis suggests that such defective growth could be the result of insufficient compression on cushions or abnormal stretch occurring in cushions during growth stages. To rectify the defects, surgical accessories may be used to apply additional compression on cushions while mitigating unnecessary tension.

Development (2021) 148, dev196519. doi:10.1242/dev.196519

In summary, this study demonstrates that osmotic stress has developmentally relevant effects on valve shape fidelity and growth. The results reveal a mechanosensitive mechanism by which compressive and tensile stresses orchestrate heart valve formation. Compressive stress promotes proliferation and inhibits the compaction phenotype via BMP signaling in coordination with MEK-ERK, while tensile stress promotes the compaction phenotype. Based on this, we proposed a growth and/or maturation switch that is controlled by mechano-regulation between BMP-, pSmad1-, pSmad5- and pSER19-mediated cell contractility. Further studies to uncover how mechanical stress coordinates underlying biomolecular mechanisms should advance our knowledge on how developmental pathways lead to the biomechanically functional morphology of heart valves.

MATERIALS AND METHODS

Avian AV cushion isolation and hanging drop culture

AV cushions (HH25) or remodeling left AV leaflets (HH36 and HH40) AV cushions were dissected from the myocardium of embryonic chick hearts. Whole tissue explants were cultured in 20 µl hanging drops, where the explant would settle at the apex (Ninomiya and Winklbauer, 2008). Control (unloaded condition) media consisted of 1×M199 (290 mOsm) with the following additives constant for all medias: 1% penicillin-streptomycin, 2.2 g/l sodium bicarbonate, 1% chick serum and 0.1% insulin-transferrin-selenium. Hypoosmotic conditions were made by supplying the same additives to 0.5×M199 (173 mOsm, −40%). Hyperosmotic media was made by adding a 0.14 M sucrose solution in control media (446 mOSM, +50%). Osmolarities were measured using a freezing point depression osmometer, calibrated using a 290 mOsm standard. Osmotic formulations were found to change stoichiometrically (linearly) with the addition or removal of solutes (Table 1).

Optical imaging of hanging drop cultures

Cushions were imaged fresh after placement in hanging drops and then again after 10 h, 18 h or 24h in culture using an upright stereo-microscope (Zeiss V20 with Retiga 4000R camera). Tissue areas were measured in FIJI (ImageJ) and the compaction ratio was computed as the ratio of final to initial area. We demonstrated that the relationship between conditions, as determined by area measurements, is the same as the relationship when measuring tissue volumes (Figs S4, S5).

Cytokines and inhibitors

The following cytokines were added to culture media: BMP2 (10 ng/ml, Krackeler Scientific), TGFβ3 (2 ng/ml, Peprotech). The following inhibitors were added to culture media: ROCK inhibitor, Y-27632 (10 µM, Cell Signaling); Alk2/3 inhibitor, LDN193189 (1 µM, Sigma); Alk 5/7 inhibitor SB431542 (2.6 µM, Sigma); MEK inhibitor, U0126 (10 µM, Sigma); and NM-myosin II inhibitor, blebbistatin (1 µM-10 µM, VWR/BioVision) (see Table S1 for details).

Left atrial ligation

Fertilized White Leghorn chicken eggs were incubated in a 38°C forced-draft incubator to Hamburger-Hamilton (HH) stage 21 (3.5 days, Hamburger and Hamilton). The embryo was cultured in an *ex vivo* platform previously described (Gould et al., 2016). Briefly, an overhand knot of 10-0 nylon suture loop was placed across a region of either the right or left atrium and tightened, partially constricting the left or right AV orifice, respectively (LAL and RAL). This diverted flow from the constricted inlet towards the untreated inlet, decreasing hemodynamic load on the one side and increasing it on the other (Boergermann et al., 2010; Aubin et al., 2004). At D7 and D10, hearts and/or AVs were fixed, and paraffin sectioned for immunofluorescence staining.

Table 1. Measured media osmolality

Formulation	Reading (mOSM/kg)	Perturbation
STRD(290)	288	Standard
Media	295	0%
Hypo-osmotic (0.5×M199 with equal buffer)	174	−41%
Hyper-osmotic (0.14 M) sucrose	446	51%

Immunofluorescence

Cushions were fixed in 4% PFA for 30 min at 4°C, permeabilized with 0.02% Triton-X and blocked using 3% BSA, 20 mM MgCl, 0.3% Tween 20, 0.3 M glycine, and 5% donkey serum in 1×TBS. Samples were incubated with the following primary antibodies at 1:100 dilution unless noted otherwise: PHH3 (mouse or rat, Cell Signaling, 9701), caspase 3 (mouse, Cell Signaling, 9662), alpha-smooth-muscleactin-Cy3 conjugated (mouse, Sigma, C6198), RhoA-GTP (mouse, New East Biosciences, 26904), Rac1-GTP (mouse, New East Biosciences, 26903), erk12pERK (rabbit, Cell Signaling, 3192), pSmad2/3 (rabbit, Cell Signaling, 9701), pSmad1/5 (Cell Signaling, 9516), pSER19 on myosin light chain kinase (rabbit, 1:50, Thermo-Scientific, PA5-17726) and VE-cadherin (rabbit, Abcam ab33168). Antibodies requiring amplification (pERK, pSmad1/5 and pSmad2/3) were also incubated in 1% H_2O_2 in PBS for 40 min, stained using HRP-conjugated secondary antibodies and incubated using a TSA kit. Secondary antibodies were applied in 5% BSA in TBS at 1:100 unless noted: goat anti-mouse Alexa Fluor 488 (Thermo, A-21202), goat anti-rabbit Alexa Fluor 568 Thermo, A11011 (1:200 for VE-cad), goat anti-mouse Alexa Fluor 635 Thermo, A31574 and donkey anti-mouse Alexa Fluor 647 A-31571. After staining, cushions were optically cleared using HISTO-M solution (Visikol). Stained cushions were imaged in glass-bottomed 96-well plates using an inverted Zeiss LSM 710 microscope. For LAL sections, whole hearts from day 7 chicks were flushed with TBS and fixed with 4% PFA overnight, embedded with paraffin wax and sectioned. Antigen retrieval was carried out with citrate buffer. Endogenous peroxidase was blocked with 1% H_2O_2 in PBS for 40 min. Sections were then permeabilized and blocked with the buffer as above. Sections were incubated with pSmad1/5 (rabbit, 1:100, Cell Signaling, 9516) or pERK12 (rabbit, 1:100, Cell Signaling, 3192) and with MF20 (mouse, 1:100, eBioscience, 14-6503-82). Sections were then incubated with donkey anti-rabbit HRP (1:100, Rockland, 611-703-127) and donkey anti-mouse AF568 (1:100, Thermo-Scientific, A10037). Signal was amplified using TSA Amplification Kit (Perkin Elmer).

Stain localization analysis

We considered each nucleus or positive cell as an object existing at a radius (r) from a centroid calculated from the location of all nuclei. This approach allows for a ROI to be defined ad hoc from the raw data, as opposed to requiring predefined segmentation steps to identify the total cushion area. The radii were then normalized on a per cushion basis by averaging the radii of M number of cells farthest from the tissue center (i.e. those with the largest radii) and dividing all radii by this average max radius R_{max}, creating r_{norm} values. This approach prevents small surface irregularities from greatly affecting normalization. With proper selection of M, this also leads to the inclusion of only surface/endothelial cells, defining a biologically reasonable condition for $r_{norm}=1$. Cells at $r_{norm}>1$ reflect deviations in the cushion size from a perfectly smooth circle. Outliers, e.g. due to another cushion at an image edge, will show up generally at $r_{norm}>1.2$. The same procedure is applied to the objects from the stain image channel to create $r_{norm,stain}$. The resulting distributions can be binned into bins of equal area by computing radii of those circles with the following formula:

$$r(i) = \sqrt{\frac{(i+1)*A_0}{\pi}},$$

where i is the circle index, with the central circle being 0, and A_0 is a selected constant area.

Statistics

Results are expressed as mean±s.e.m., with $n \geq 4$ independent cultures per treatment condition and four- to six-dozen chick embryos pooled for each

experiment. Statistical analysis was carried out using SAS and/or Excel software. Treatment effects were compared using either an ANOVA with Tukey post-hoc paired tests or a *t*-test, and data were transformed when necessary to obtain equal sample variances. Differences between means were considered significant at $P \leq 0.05$.

Acknowledgements
Confocal imaging was supported by NYSTEM C029155 and NIH S10OD018516 funding for the Zeiss LSM880 microscopes (i880 and u880).

Competing interests
The authors declare no competing or financial interests.

Author contributions
Conceptualization: D.M.B., D.P., J.B.; Methodology: D.M.B., D.P., R.S.; Software: D.M.B.; Validation: S.S.; Investigation: D.M.B., M.W., D.P., S.S., R.R., R.S.; Resources: J.B.; Data curation: D.M.B.; Writing - original draft: D.M.B.; Writing - review & editing: D.M.B., M.W., R.R., J.B.; Visualization: D.M.B., M.W., D.P., S.S.; Supervision: D.M.B., M.W., D.P., J.B.; Funding acquisition: J.B.

Funding
This research was supported by federal grants from the National Institutes of Health (HL110328 and HL128745) and the National Science Foundation (CMMI-1635712 and a Graduate Research Fellowship Program award to D.M.B.). Deposited in PMC for release after 12 months.

Peer review history
The peer review history is available online at https://journals.biologists.com/dev/article-lookup/doi/10.1242/dev.196519

References
Ahsan, S., Ge, Y. and Tainsky, M. A. (2016). Combinatorial therapeutic targeting of BMP2 and MEK-ERK pathways in NF1-associated malignant peripheral nerve sheath tumors. *Oncotarget* **7**, 57171-57185. doi:10.18632/oncotarget.11036

Aikawa, E., Whittaker, P., Farber, M., Mendelson, K., Padera, R. F., Aikawa, M. and Schoen, F. J. (2006). Human semilunar cardiac valve remodeling by activated cells from fetus to adult: implications for postnatal adaptation, pathology, and tissue engineering. *Circulation* **113**, 1344-1352. doi:10.1161/CIRCULATIONAHA.105.591768

Aubin, J., Davy, A. and Soriano, P. (2004). In vivo convergence of BMP and MAPK signaling pathways: impact of differential Smad1 phosphorylation on development and homeostasis. *Genes Dev.* **18**, 1482-1494. doi:10.1101/gad.1202604

Basser, P. J., Schneiderman, R., Bank, R. A., Wachtel, E. and Maroudas, A. (1998). Mechanical properties of the collagen network in human articular cartilage as measured by osmotic stress technique. *Arch. Biochem. Biophys.* **351**, 207-219. doi:10.1006/abbi.1997.0507

Beppu, H., Malhotra, R., Beppu, Y., Lepore, J. J., Parmacek, M. S. and Bloch, K. D. (2009). BMP type II receptor regulates positioning of outflow tract and remodeling of atrioventricular cushion during cardiogenesis. *Dev. Biol.* **331**, 167-175. doi:10.1016/j.ydbio.2009.04.032

Boergermann, J. H., Kopf, J., Yu, P. B. and Knaus, P. (2010). Dorsomorphin and LDN-193189 inhibit BMP-mediated Smad, p38 and Akt signalling in C2C12 cells. *Int. J. Biochem. Cell Biol.* **42**, 1802-1807. doi:10.1016/j.biocel.2010.07.018

Buskohl, P. R., Jenkins, J. T. and Butcher, J. T. (2012a). Computational simulation of hemodynamic-driven growth and remodeling of embryonic atrioventricular valves. *Biomech. Model. Mechanobiol.* **11**, 1205-1217. doi:10.1007/s10237-012-0424-5

Buskohl, P. R., Sun, M. L., Thompson, R. P. and Butcher, J. T. (2012b). Serotonin potentiates transforming growth factor-beta3 induced biomechanical remodeling in avian embryonic atrioventricular valves. *PLoS ONE* **7**, e42527. doi:10.1371/journal.pone.0042527

Butcher, J. T., Norris, R. A., Hoffman, S., Mjaatvedt, C. H. and Markwald, R. R. (2007). Periostin promotes atrioventricular mesenchyme matrix invasion and remodeling mediated by integrin signaling through Rho/PI 3-kinase. *Dev. Biol.* **302**, 256-266. doi:10.1016/j.ydbio.2006.09.048

Chevalier, N. R., Gazguez, E., Dufour, S. and Fleury, V. (2016). Measuring the micromechanical properties of embryonic tissues. *Methods* **94**, 120-128. doi:10.1016/j.ymeth.2015.08.001

Gilboa, S. M., Devine, O. J., Kucik, J. E., Oster, M. E., Riehle-Colarusso, T., Nembhard, W. N., Xu, P., Correa, A., Jenkins, K. and Marelli, A. J. (2016). Congenital heart defects in the United States: estimating the magnitude of the affected population in 2010. *Circulation* **134**, 101-109. doi:10.1161/CIRCULATIONAHA.115.019307

Gould, R. A., Yalcin, H. C., Mackay, J. L., Sauls, K., Norris, R., Kumar, S., Butcher, J. T., Gould, R. A., Yalcin, H. C., Mackay, J. L. et al. (2016). Cyclic mechanical loading is essential for Rac1-mediated elongation and remodeling of the embryonic mitral valve. *Curr. Biol.* **26**, 27-37. doi:10.1016/j.cub.2015.11.033

Hoffman, J. I. E. (2013). The global burden of congenital heart disease. *Cardiovasc. J. Afr.* **24**, 141-145. doi:10.5830/CVJA-2013-028

Hove, J. R., Köster, R. W., Forouhar, A. S., Acevedo-Bolton, G., Fraser, S. E. and Gharib, M. (2003). Intracardiac fluid forces are an essential epigenetic factor for embryonic cardiogenesis. *Nature* **421**, 172-177. doi:10.1038/nature01282

Hughes, A. J., Miyazaki, H., Coyle, M. C., Zhang, J., Laurie, M. T., Chu, D., Vavrušová, Z., Schneider, R. A., Klein, O. D. and Gartner, Z. J. (2018). Engineered tissue folding by mechanical compaction of the mesenchyme. *Dev. Cell* **44**, 165-178.e6. doi:10.1016/j.devcel.2017.12.004

Jackson, L. F., Qiu, T. H., Sunnarborg, S. W., Chang, A., Zhang, C., Patterson, C. and Lee, D. C. (2003). Defective valvulogenesis in HB-EGF and TACE-null mice is associated with aberrant BMP signaling. *EMBO J.* **22**, 2704-2716. doi:10.1093/emboj/cdg264

Kain, K. H., Miller, J. W. I., Jones-Paris, C. R., Thomason, R. T., Lewis, J. D., Bader, D. M., Barnett, J. V. and Zijlstra, A. (2014). The chick embryo as an expanding experimental model for cancer and cardiovascular research. *Dev. Dyn.* **243**, 216-228. doi:10.1002/dvdy.24093

Lindsey, S. E., Butcher, J. T. and Yalcin, H. C. (2014). Mechanical regulation of cardiac development. *Front. Physiol.* **5**, 318. doi:10.3389/fphys.2014.00318

Ma, L., Lu, M.-F., Schwartz, R. J. and Martin, J. F. (2005). Bmp2 is essential for cardiac cushion epithelial-mesenchymal transition and myocardial patterning. *Development* **132**, 5601-5611. doi:10.1242/dev.02156

MacGrogan, D., D'Amato, G., Travisano, S., Martinez-Poveda, B., Luxán, G., Del Monte-Nieto, G., Papoutsi, T., Sbroggio, M., Bou, V., Gomez-Del Arco, P. et al. (2016). Sequential ligand-dependent notch signaling activation regulates valve primordium formation and morphogenesis. *Circ. Res.* **118**, 1480-1497. doi:10.1161/CIRCRESAHA.115.308077

Midgett, M. and Rugonyi, S. (2014). Congenital heart malformations induced by hemodynamic altering surgical interventions. *Front. Physiol.* **5**, 287. doi:10.3389/fphys.2014.00287

Ninomiya, H. and Winklbauer, R. (2008). Epithelial coating controls mesenchymal shape change through tissue-positioning effects and reduction of surface-minimizing tension. *Nat. Cell Biol.* **10**, 61-69. doi:10.1038/ncb1669

Nishimura, R. A., Otto, C. M., Bonow, R. O., Carabello, B. A., Erwin, J. P., III, Guyton, R. A., O'Gara, P. T., Ruiz, C. E., Skubas, N. J., Sorajja, P. et al. (2014). 2014 AHA/ACC guideline for the management of patients with valvular heart disease: executive summary: a report of the American college of cardiology/American heart association task force on practice guidelines. *Circulation* **129**, 2440-2492. doi:10.1161/CIR.0000000000000029

Rivera-Feliciano, J. and Tabin, C. J. (2006). Bmp2 instructs cardiac progenitors to form the heart-valve-inducing field. *Dev. Biol.* **295**, 580-588. doi:10.1016/j.ydbio.2006.03.043

Sedmera, D., Pexieder, T., Rychterova, V., Hu, N. and Clark, E. B. (1999). Remodeling of chick embryonic ventricular myoarchitecture under experimentally changed loading conditions. *Anat. Rec.* **254**, 238-252. doi:10.1002/(SICI)1097-0185(19990201)254:2<238::AID-AR10>3.0.CO;2-V

Srivastava, D. (2006). Making or breaking the heart: from lineage determination to morphogenesis. *Cell* **126**, 1037-1048. doi:10.1016/j.cell.2006.09.003

Van Der Linde, D., Konings, E. E. M., Slager, M. A., Witsenburg, M., Helbing, W. A., Takkenberg, J. J. M. and Roos-Hesselink, J. W. (2011). Birth prevalence of congenital heart disease worldwide: a systematic review and meta-analysis. *J. Am. Coll. Cardiol.* **58**, 2241-2247. doi:10.1016/j.jacc.2011.08.025

Virani, S. S., Alonso, A., Benjamin, E. J., Bittencourt, M. S., Callaway, C. W., Carson, A. P., Chamberlain, A. M., Chang, A. R., Cheng, S., Delling, F. N. et al. (2020). Heart disease and stroke statistics—2020 update: a report from the American heart association. *Circulation* **141**, e139-e596. doi:10.1161/CIR.0000000000000757

Wang, J., Liu, S., Heallen, T. and Martin, J. F. (2018). The Hippo pathway in the heart: pivotal roles in development, disease, and regeneration. *Nat. Rev. Cardiol.* **15**, 672-684. doi:10.1038/s41569-018-0063-3

Yalcin, H. C., Shekhar, A., McQuinn, T. C. and Butcher, J. T. (2011). Hemodynamic patterning of the avian atrioventricular valve. *Dev. Dyn.* **240**, 23-35. doi:10.1002/dvdy.22512

Zhou, J., Lee, P.-L., Lee, C.-I., Wei, S.-Y., Lim, S. H., Lin, T.-E., Chien, S. and Chiu, J.-J. (2013). BMP receptor-integrin interaction mediates responses of vascular endothelial Smad1/5 and proliferation to disturbed flow. *J. Thromb. Haemost.* **11**, 741-755. doi:10.1111/jth.12159

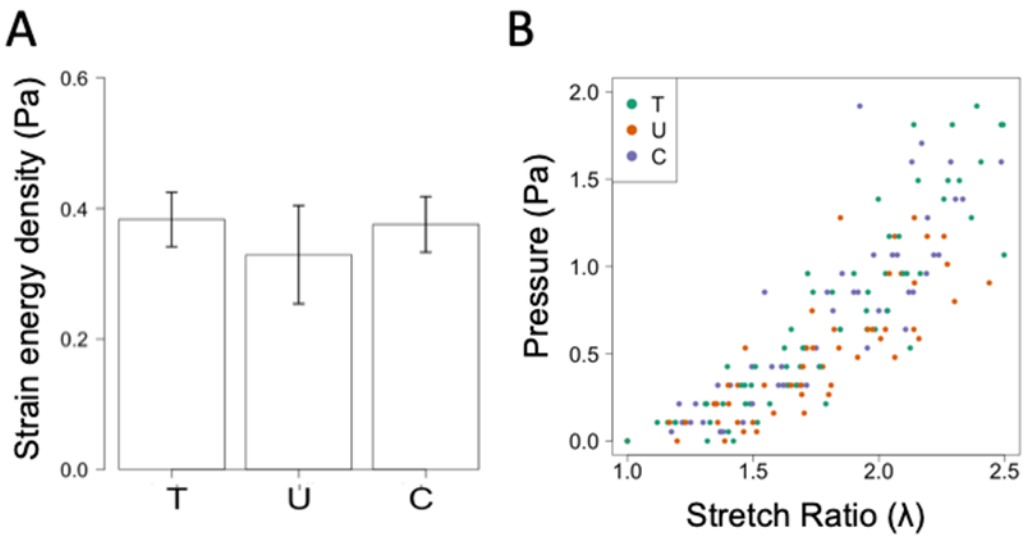

Figure S1. Osmotic stress does not alter tissue stiffness. (A) Micropipette aspiration measurements of strain energy density, (B) Mechanical response curves for the cushions tested n = 5-6 cushions per condition per 3 independent experiments, SEM shown.

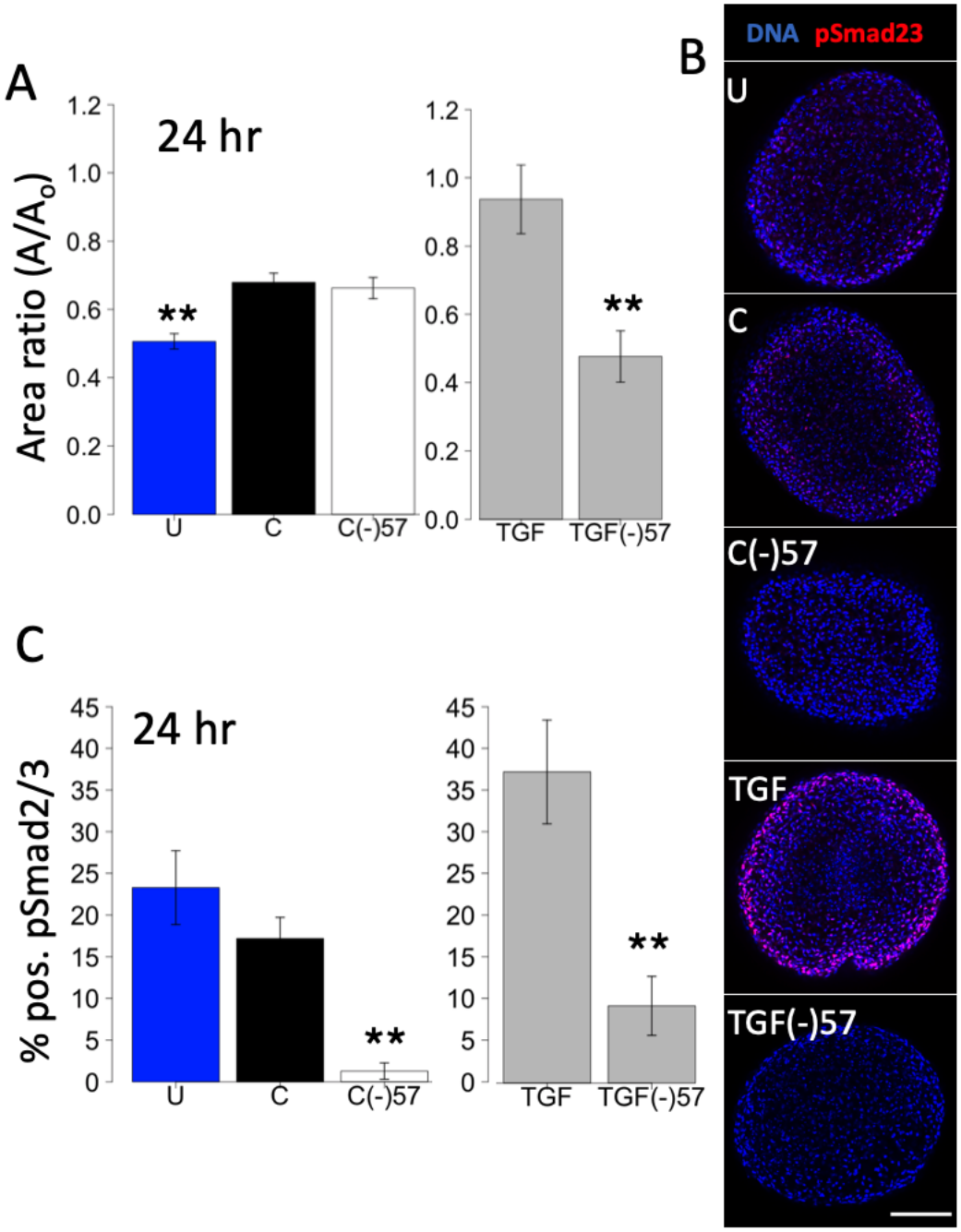

Figure S2. Osmotic stress compaction phenotype is pSmad2/3 independent. (A) Compaction trend at 24hrs ** $p < 0.005$ between conditions (B) Number of cells positive for pSmad2/3 at 24hrs (D) Whole mount IF images of 24 hr. cushions stained for pSmad2/3, scale bar 100uM, n=6-8 cushions per conditions, SD shown.

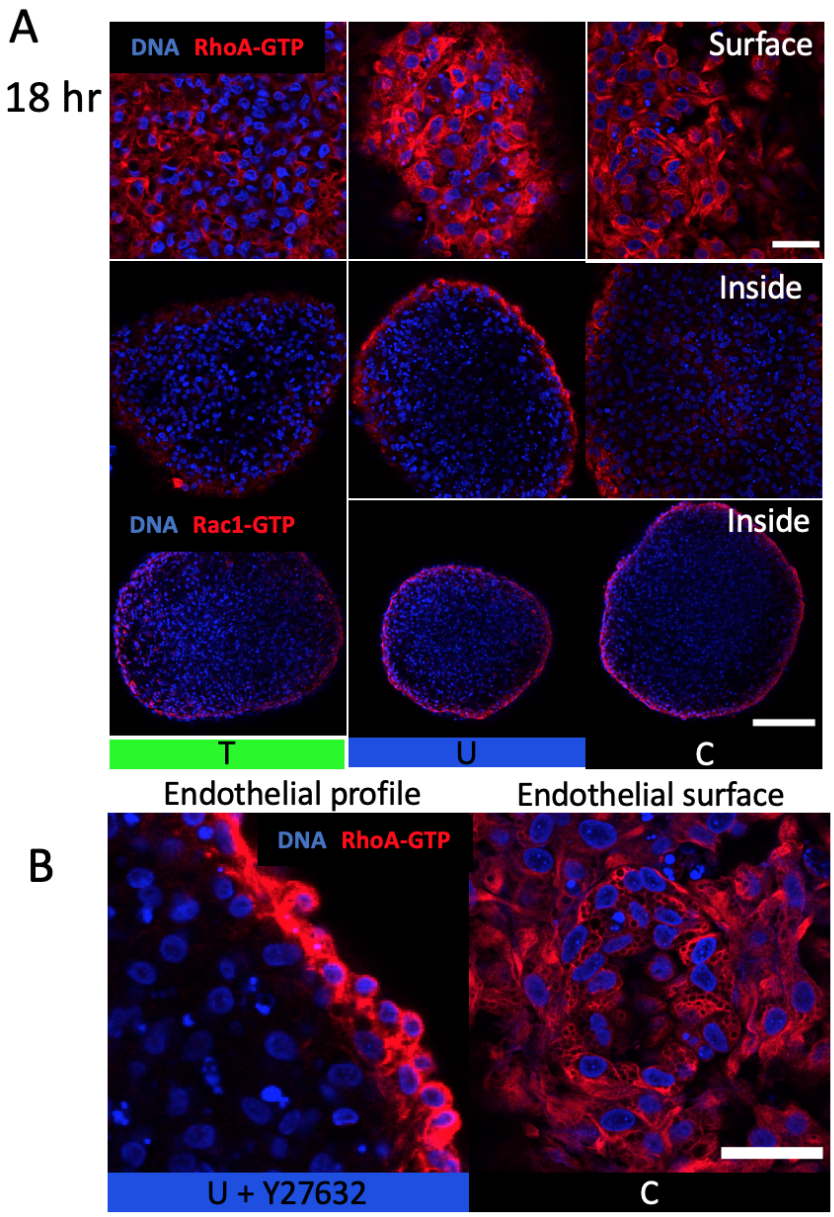

Figure S3. Osmotic stress affects endothelial RhoA-GTP patterning not activity. (A) RhoA-GTP localization on cushion surface and 30 microns inside and Rac1-GTP inside (B) Disruption of apical-basal polarity at endothelium with ROCK inhibition (C) Honeycomb like pattern in RhoA-GTP stain associated with compressive stress

Evaluation of 2D and 3D compaction

Cushion area can be measured from a single image of a live cushion and captures the relationship between treatment conditions without requiring measurements orthogonal to the imaging plane. Figure S4 demonstrates that using either an area ratio (Fig. S4A) or volume ratio (Fig. S4B), the relationship between conditioned medias is preserved.

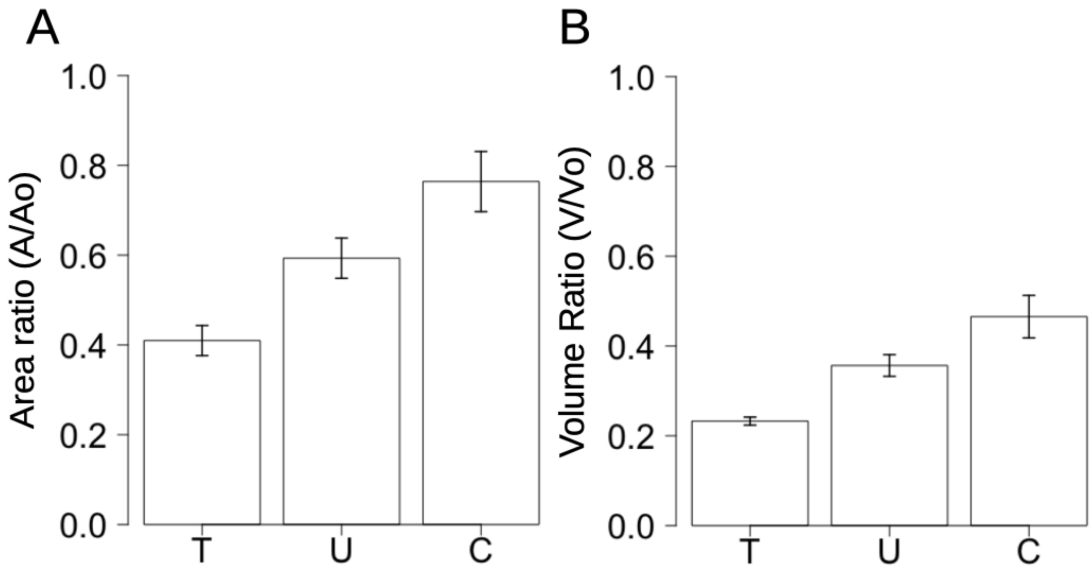

Figure S4. Area and volumetric compaction of HH25 cushions yield the same relationship between conditioned medias. (A) Area ratios comparing cushion areas at 0hrs and 24hrs. (B) Volume ratios comparing cushion volumes at 0hrs and 24hrs. T = Tensile stress, U = Unloaded, C = Compressive stress.

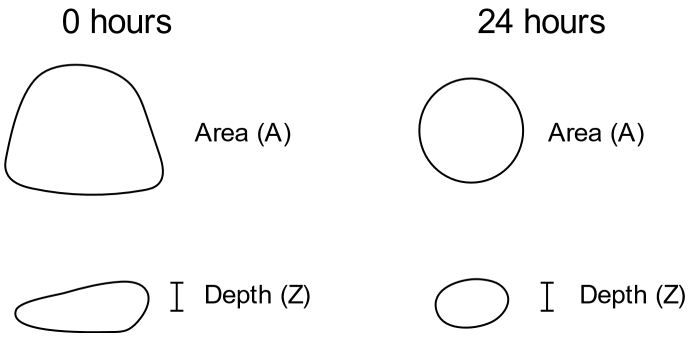

Figure S5. Schematic of HH25 cushion morphologies at 0 and 24 hours of culture

To approximate the volume of live cushions, cushion height was measured by comparing the microscope Z-position when focused on the top-most surface of the cushion and the centerline of the cushion. Volumetric compaction of HH25 cushions was calculated using two different approximations for volume at t = 0 hours and t = 24 hours. At the initial time point, the cushions are flatter and their upper volume was approximated as their 2D area (A) multiplied by their calculated thickness (Z) as represented in Figure S4:

$$\frac{V_o}{2} = A_o Z_o$$

At the 24-hour time point, however, cushions form an ellipsoid. While the volume of an ellipsoid is given by $V = \frac{4}{3}\pi abc$, where a, b, and c represent the axial radii, compacted HH25 cushions have relatively similar radii on their x- and y-planes under a microscope. As a result, the formula can be simplified to:

$$V_f = \frac{4}{3}\pi abc = \frac{4}{3}\pi r^2 Z_f$$

$$\frac{V_f}{2} = \frac{2}{3} A_f Z_f$$

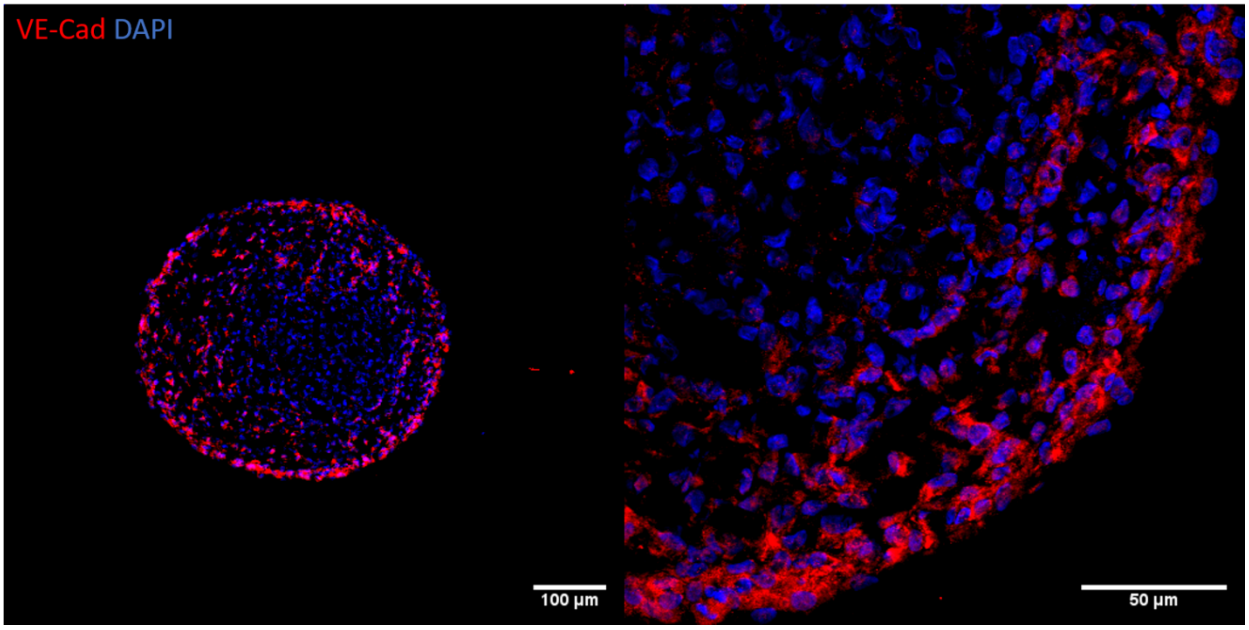

Figure S6. VE-Cadherin labeling shows most endothelial cells remained on the surface of cushions.

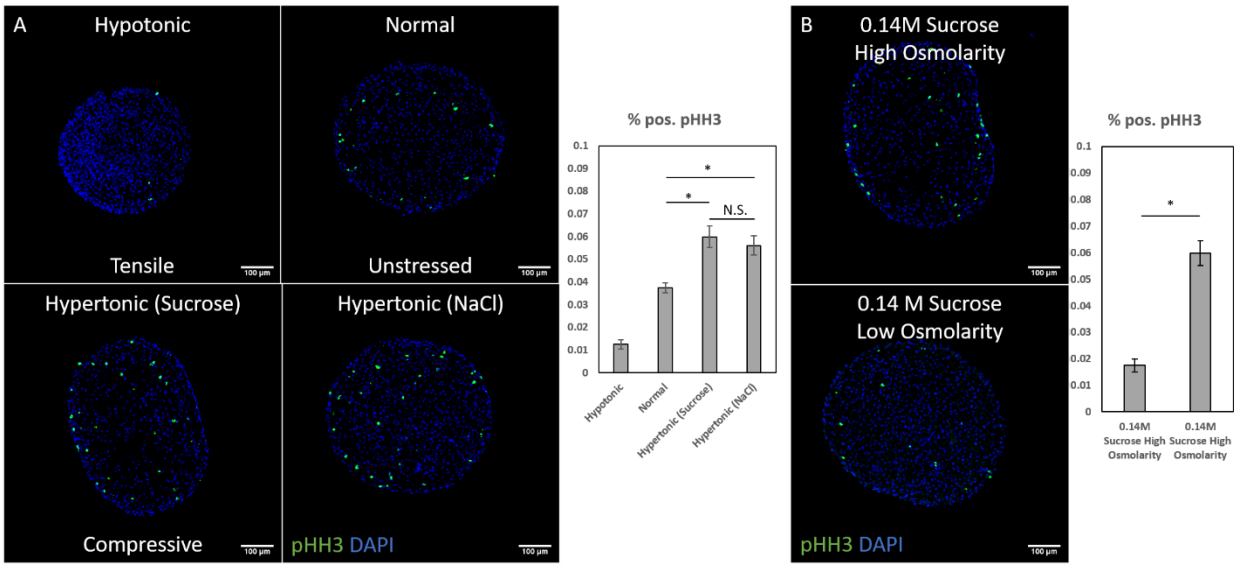

Figure S7. Addition of sucrose did not have a significant impact on cell proliferation. (A) Representative IF images of pHH3 in HH25 cushions cultured under osmotic stress for 24 hours, and quantification of pHH3 positive cells, n = 4-5, SD shown. (B) Representative IF images of pHH3 in HH25 cushions cultured in media with the same amount of sucrose added but different osmolarity for 24 hours, and quantification of pHH3 positive cells, n = 4-5, SD shown.

Table S1. Cytokines and inhibitors

Target	Name	Concentration	Provider	Dosage reference
ROCK	Y-27632	10 μM	Cell Signaling	(Gould et al., 2016)
Alk2/3	LDN193189	1 μM	Sigma	(Ahsan et al., 2016; Boergermann et al., 2010)
Alk 5/7	SB431542	2.6 μM	Sigma	(Buskohl et al., 2012a,b)
MEK	U0126	10 μM	Sigma	(Aubin et al., 2004)
NM-Myosin II	(+-) Blebbistatin	1 μM-10 μM	VWR BioVision	Manufacture solubility and empirical titration